Periodic structures in a 2D lattice with competing interactions and a ϕ^4 substrate

1990 J. Phys. A: Math. Gen. 23 225

(http://iopscience.iop.org/0305-4470/23/2/018)

J. Phys. A: Math. Gen. 23 (1990) 225-240. Printed in the UK

Periodic structures in a 2D lattice with competing interactions and a φ^4 substrate

G Vlastou-Tsinganos†, N Flytzanis† and H Büttner‡

† Physics Department, University of Crete, Heraklion, Greece

‡ Physikalisches Institute, Universitat Bayreuth, D-8580 Bayreuth, Federal Republic of Germany

Received 4 November 1988, in final form 30 June 1989

Abstract. We study a 2D triagonal lattice with competing first- and second-neighbour harmonic interactions and a φ^4 on-site potential. At zero temperature we determine the classical ground-state configurations of low periodicity. The phase diagram in the interaction parameter space is significantly different from that calculated for the piecewise quadratic on-site potential. The main difference is in the phonon stability regions of the different periodicities.

1. Introduction

Crystal polytypes (Behnke *et al* 1986) and incommensurate structures (Janssen and Tjon 1982, Jannsen 1986a) often result from the competition of different interactions of an atom or an Ising spin with its environment. An extensively studied model which presents the competition between two different ordering mechanisms (the substrate potential and the interatomic interactions of the overlying atomic chain) is the 1D Frenkel-Kontorova model. While it was originally constructed as a prototype to study plastic deformation, it has been used to study commensurate-incommensurate phase transitions (Aubry 1979, Bak 1982) in one dimension.

In another context, a bistable on-site potential is an important ingredient in the description of perovskite ferroelectrics. In this model the nonlinear potential is between an ion and its electronic shell. It is usually assumed to be a φ^4 potential which simulates the strong anharmonic polarisability of the O^{2-} ion, an important element in most perovskites (Bilz *et al* 1987).

The anharmonic φ^4 bistable potential has a smooth maximum at zero and is steep for large arguments, so that it is energetically unfavourable to move to large displacements. This on-site potential is often approximated by a double quadratic (DQ) potential, as in the study of the frustration due to the competing elastic constants for first- and second-neighbour interactions, in a 1D chain or a 2D structure (Axel and Aubry 1981, Büttner and Heym 1987). Its important advantage is that almost all the mathematical problems can be solved analytically. Its drawbacks, as a physical model, are the discontinuity in the force at zero displacement and the behaviour for large displacements. The first can be remedied by introducing a piecewise quadratic potential which can be treated self-consistently by simple eigenvalue techniques and using the solution of the DQ as a 'Green function' for the problem (Flytzanis *et al* 1979).

0305-4470/90/020225+16$03.50

Extensive work in various nonlinear lattice models has been done by Bilz, Büttner and co-workers (Bilz *et al* 1980, Behnke and Büttner 1982) in one-dimensional models, and in a few two-dimensional square lattices including anisotropy. In 2D models the on-site potential is doubly quadratic. The φ^4 model, due to its difficulty in analytic computations, has been studied only in 1D (Frosch and Büttner 1985). It is of interest therefore to extend these results to 2D.

It should also be remarked that the double-well-type potentials present many similarities to the Ising models (Katsura *et al* 1986) but also some differences which will be mentioned in the discussion. Also results from classical planar XY models and 2D classical Heisenberg models show a significant correspondence with the results from anharmonic bistable on-site potentials. A similar problem of current interest is the formation of noble-gas monolayers on a graphite substrate which can be modelled by a φ^4 potential (Gordon and Villain 1985).

In this paper we study the classical static configurations for a triagonal planar lattice at zero temperature with first- and second-neighbour interactions and a φ^4 on-site potential perpendicular to the plane. The displacements are perpendicular to the plane and the interaction parameters are such that we are in the displacive limit. The results will be compared with recent calculations for a DQ on-site potential (Büttner and Heym 1987). The above results can also be relevant to surface reconstruction (Kanamori and Okamoto 1985) as in the [111] silicon surface where the 7×7 reconstruction is caused mainly by a perpendicular movement of the surface atoms and the appearance of adatoms to saturate dangling bonds (Takayanagi *et al* 1985). The model may also represent a molecular group (or a magnetic atom) centred on fixed lattice sites but free to rotate about these sites. It can also describe a rotating BX_4 tetrahedron in the family of A_2BX_4 compounds (Janssen 1986b) or an octahedron (NbO_6) in a $Ba_2NaNb_5O_{15}$ film (Srolovitz and Scott 1986). In the order-disorder limit one can find the degenerate ground states and define an appropriate clock model (Srolovitz and Scott 1986) which simplifies the calculations.

The paper is organised as follows. In section 2, we present the model and some simple analytical solutions. In section 3 we determine the phase diagram and compare different potentials, while in section 4 we examine the stability of the different periodic configurations. In the last section we summarise and discuss our results.

2. The nonlinear lattice model

We consider a two-dimensional triagonal lattice with atomic displacements $u_{n,m}$ normal to the surface, where (n, m) locate the lattice points on the skew coordinate system shown in figure 1(a), in the x and y directions respectively. The Hamiltonian of the system is

$$H = \frac{1}{2}\sum_{n,m}\{M\dot{u}_{n,m}^2 + f_1[(u_{n+1,m}-u_{n,m})^2 + (u_{n,m+1}-u_{n,m})^2 + (u_{n-1,m+1}-u_{n,m})^2] + f_2[(u_{n+1,m-2}-u_{n,m})^2 + (u_{n+2,m-1}-u_{n,m})^2 + (u_{n+1,m+1}-u_{n,m})^2]\} + \sum_{n,m} V(u_{n,m}) \tag{1}$$

where f_1 and f_2 are the interaction parameters with the first and second neighbour. $V(u_{n,m})$ is the bistable on-site potential given for the φ^4 model by

$$V(u_{n,m}) = \tfrac{1}{4}g_4(u_{n,m}^2 - g_0/g_4)^2 \tag{2}$$

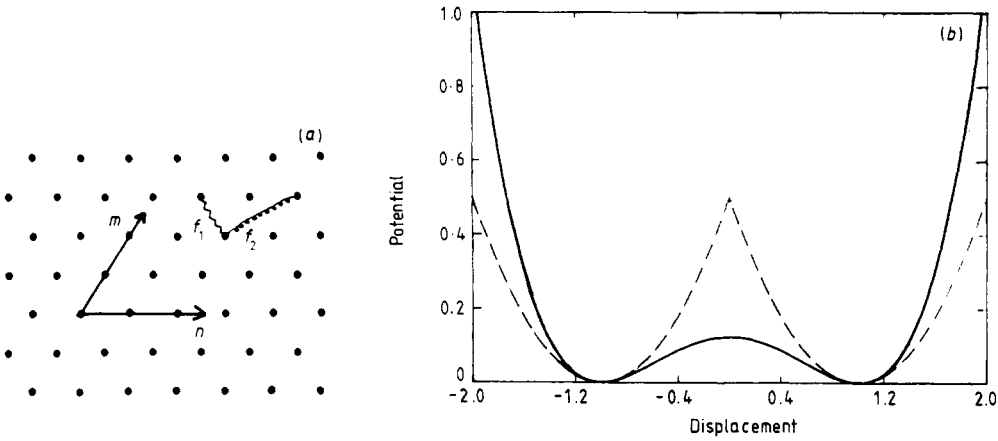

Figure 1. (*a*) Triagonal lattice. (*b*) Plot of the φ^4 potential (full line) for $g_0 = 0.5$, $g_4 = 0.5$ and double quadratic potential (broken line) with $\sigma = 1$, $k^2 = 1$.

with $g_0, g_4 > 0$, and for the DQ by

$$V(u_{n,m}) = \tfrac{1}{2}k^2(u_{n,m} - \sigma_{n,m})^2 \tag{3}$$

with $\sigma_{n,m} = \sigma_0 \operatorname{sgn}(u_{n,m})$ and σ_0 is the position of the potential minimum. In what follows we consider the φ^4 potential and make comparisons with the results for the DQ potential (Büttner and Heym 1987). The mass M can be easily scaled out by choosing appropriate units. Here for simplicity (but without losing generality) we chose $M = 1$.

The important physical parameters of the φ^4 (DQ) potential are the position of the minima $u_0 = \sqrt{g_0/g_4}$ ($u_0 = \sigma_0$), the barrier height $E_0 = g_0^2/4g_4$ ($E_0 = k^2\sigma_0^2/2$) and the frequency of oscillation $\omega_0^2 = 2g_0$ ($\omega_0^2 = k^2$) near the minima. Since both potentials (φ^4 and DQ) have only two parameters, we can equate only two of the above physical quantities. In comparing the two potentials for displacements near the minima we have to fix u_0 and ω_0, while for large displacements it is more appropriate to fix u_0 and the potential barrier E_0. For simplicity we have chosen the former which is appropriate for small f_1 and f_2. Then we can eliminate one of the parameters (g_0 or k^2) by normalising all the interatomic force constants to ω_0^2. So, we can write

$$c_1 = f_1/2g_0 \qquad c_2 = f_2/2g_0 \qquad \text{for } \varphi^4 \tag{4a}$$

$$c_1 = f_1/k^2 \qquad c_2 = f_2/k^2 \qquad \text{for DQ.} \tag{4b}$$

This normalisation is used in presenting the phase diagrams. To compare the two potentials for large f_1 and f_2, where the potential barrier is important, we must normalise them to $g_0/2$ and not to $2g_0$ for the φ^4 potential, since E_0 is fixed. In giving the different analytic formulae, however, we have kept f_1 and f_2 explicitly. In what follows we choose $k^2 = 1$ and $\sigma_0 = 1$ for the DQ potential and $g_0 = g_4 = 0.5$ for the φ^4 potential. In fact the results can be extended to any value of g_4 for the φ^4 model, if we measure displacements in units of $\sqrt{g_0/g_4}$, force constants in units of g_0, so that the energy is measured in units of g_0/g_4 and g_4 is thus eliminated.

Since c_1 (or f_1) and c_2 (or f_2) can be either positive or negative, a competition can arise between neighbouring interactions, while the local potential tends to lock the system. Thus, we expect a variety of possible ground states at zero temperature ($T = 0$).

They can be obtained as static solutions of the following nonlinear difference equation:

$$\ddot{u}_{n,m} = f_1 \Delta_6 u_{n,m} + f_2 \Delta_6' u_{n,m} + g_0 u_{n,m} - g_4 u_{n,m}^3 = 0 \tag{5}$$

where the difference operators Δ_6 and Δ_6' are defined as:

$$\Delta_6 u_{n,m} = u_{n+1,m} + u_{n,m+1} + u_{n-1,m+1} + u_{n-1,m} + u_{n,m-1} + u_{n+1,m-1} - 6u_{n,m} \tag{6a}$$

$$\Delta_6' u_{n,m} = u_{n+1,m-2} + u_{n+2,m-1} + u_{n+1,m+1} + u_{n-1,m+2} + u_{n-2,m+1} + u_{n-1,m-1} - 6u_{n,m}. \tag{6b}$$

For the DQ case the force is given by

$$-k^2[u_{n,m} - \sigma_0 \operatorname{sgn}(u_{n,m})].$$

There is a large number of solutions to these equations, but here we will only be interested in commensurate states. In general, the solutions for the φ^4 potential must be obtained numerically but for some special cases we can obtain simple analytic solutions, such as the following two obvious cases. (i) The $N \times 1$ (N = even) configuration where the displacement u is only a function of n and is the same for all m. It has $N/2$ up and $N/2$ down displacements symmetrically having equal absolute displacements. Equivalently the displacement can depend only on m, $1 \times M$ configuration, which is degenerate in energy with $N \times 1$ for $N = M$. (ii) The $N \times 1$ (N = odd) configuration of $(N+1)/2$ up and $(N-1)/2$ down, with some equal absolute displacements. Of course there are other solutions depending on n and m simultaneously, while there is also the possibility of symmetry breaking by spontaneous creation of domains. In table 1 we present the analytic solutions obtained with the φ^4 potential for the displacements and energy. In table 2 we present the corresponding results for the DQ potential. In reading table 2 we must be careful that in the variation of the parameters f_1 and f_2 the denominators in the displacements remain positive. This is consistent with the choices for the $\sigma_{n,m}$ or equivalently the sign of $u_{n,m}$. By expanding the formulae for small f_1 and f_2 for $k^2 = 2g_0$ one can easily show that the results for the φ^4 and DQ potentials are identical. For the more general periodicities we must use numerical techniques and the results are described in the next section.

In section 4 we will examine the phonon stability of these solutions but one remark can already be made by looking at the 2×1 structure for the two cases. In the DQ case the vanishing of the denominator in the displacement (and in energy) means that near

Table 1. Analytic solutions for the displacements and energy, obtained with the φ^4 potential.

Period	Structure	Displacement	Energy/site	Conditions
1×1	↑	$\pm\sqrt{g_0/g_4}$	0	$g_0 > 0$
2×1	↑ ↓	$\pm\dfrac{\sqrt{g_0 - 8(f_1+f_2)}}{\sqrt{g_4}}$	$-\dfrac{1}{4g_4}[g_0 - 8(f_1+f_2)]^2 + \dfrac{g_0^2}{4g_4}$	$g_0 - 8(f_1+f_2) > 0$
3×1(D)	↑ • ↓	$0, \pm\dfrac{\sqrt{g_0 - 6f_1 - 9f_2}}{\sqrt{g_4}}$	$-\dfrac{1}{6g_4}[g_0 - 6f_1 - 9f_2]^2 + \dfrac{g_0^2}{4g_4}$	$g_0 - 6f_1 - 9f_2 > 0$
4×1	↑ ↑ ↓ ↓	$\pm\dfrac{\sqrt{g_0 - 4f_1 - 8f_2}}{\sqrt{g_4}}$	$-\dfrac{1}{4g_4}[g_0 - 4f_1 - 8f_2]^2 + \dfrac{g_0^2}{4g_4}$	$g_0 - 4f_1 - 8f_2 > 0$
3×3(D)	↑ ↓ • ↓ • ↑ • ↑ ↓	$0, \pm\dfrac{\sqrt{g_0 - 9f_1}}{\sqrt{g_4}}$	$-\dfrac{1}{6g_4}[g_0 - 9f_1]^2 + \dfrac{g_0^2}{4g_4}$	$g_0 - 9f_1 > 0$

Table 2. Analytic solutions for the displacements and energy, obtained with the DQ potential

Period	Structure	Displacement	Energy/site	Conditions
1×1	$\uparrow$	$\pm\sigma_0$	0	$u>0$
2×1	$\uparrow\downarrow$	$\pm\dfrac{k^2\sigma_0}{k^2+8(f_1+f_2)}$	$\dfrac{4k^2\sigma_0^2(f_1+f_2)}{k^2+8(f_1+f_2)}$	$k^2+8(f_1+f_2)>0$
3×1(D)	$\uparrow\bullet\downarrow$	$0,\pm\dfrac{k^2\sigma_0}{k^2+6f_1+9f_2}$	$\dfrac{k^2\sigma_0^2(6f_1+9f_2)}{k^2+6f_1+9f_2}$	$k^2+6f_1+9f_2>0$
4×1	$\uparrow\uparrow\downarrow\downarrow$	$\pm\dfrac{k^2\sigma_0}{k^2+4f_1+8f_2}$	$\dfrac{2k^2\sigma_0^2(f_1+2f_2)}{k^2+4f_1+8f_2}$	$k^2+4f_1+8f_2>0$
3×3(D)	$\uparrow\downarrow\bullet$ $\downarrow\bullet\uparrow$ $\bullet\uparrow\downarrow$	$0,\pm\dfrac{k^2\sigma_0}{k^2+9f_1}$	$\dfrac{3k^2\sigma_0^2f_1}{k^2+9f_1}$	$k^2+9f_1>0$
3×3	$\uparrow\uparrow\downarrow$ $\uparrow\downarrow\uparrow$ $\downarrow\uparrow\uparrow$	$\sigma_0\dfrac{k^2-3f_1}{k^2+9f_1}$ $-\sigma_0\dfrac{k^2+3f_1}{k^2+9f_1}$	$\dfrac{4k^2\sigma_0^2f_1}{k^2+9f_1}$	$k^2+9f_1>0$

$8(f_1+f_2)+k^2=0$ the atoms have very large potential energy from the on-site potential, which is balanced by the competitive interactions between neighbours. The corresponding instability for the φ^4 potential comes from the vanishing of the argument in the square root for the displacement, corresponding to the two atoms moving opposite towards the top of the barrier.

3. Numerical evaluation of ground states

To determine the phase diagram in the space of the parameters c_1 and c_2, for the low periodicities, we use the method of simulated annealing, in order to minimise the energy (Kirkpatrick *et al* 1983). The idea is in analogy with crystal annealing with heating and slow cooling allowing enough time for the redistribution of atoms as they lose mobility. This fictitious heating and cooling, i.e. the pattern used, is critical for the correct determination of the low-energy state. It uses a Boltzmann probability distribution function, which allows even at low temperature a small chance of a system being a high-energy state. Therefore, there is a corresponding chance for the system to get out of a local energy minimum in favour of finding a more global one. Starting with a certain $n\times1$ or $n\times m$ unit cell with random displacement coordinates, but with periodic boundary conditions, we lower the energy by the above Monte Carlo method. Using the appropriate annealing pattern, we locate the global minimum approximate configuration. We then proceed to find the exact energy minimum by fine tuning with the gradient method, using the energy derivative to ensure the correct direction of minimisation. It is impossible to give an exact recipe for the annealing pattern. What is important in this procedure is to make it easy for configuration changes to climb over energy barriers, so that it visits all the local minima. A characteristic pattern is given below, but in each case one must make sample runs to choose initial temperature, cooling rate, sampling pattern and atomic displacement, to make sure that all possible

low-energy configurations are visited. The highest fictitious temperature was usually taken as about the barrier height for the φ^4 potential, which in dimensionless units is equal to $\frac{1}{8}$. For small f_1 and f_2 (or competing) this has been checked to be sufficient so that we visit many times the possible configurations. In general, with 20 steps we lower the fictitious temperature just above zero, so that we can still visit all nearby minima, while the global minimum is left to be found by the gradient method. For each temperature we use at least 10 000 points subdivided into 100 groups of 100 points, to locate the minimum more reliably. The maximum random atomic displacements were varied between 0.1 and 0.3. The results were also repeated with different initial conditions. Using large atomic displacements can be very efficient to overcome barriers. The exact annealing pattern varies for different regions in the c_1, c_2 parameter space, depending on whether one expects high barriers in configuration space or very closely spaced minima. For example, the region where the $n \times 1$ periodicities are found is one example where the global minimum of the configuration is very close to other minima and so for its determination one must be very careful. So one might have to change the maximum temperature, number of temperature steps, cooling rate, displacement, etc.

The phase diagram in figure 2, made with the above techniques, shows the following periodic configurations to dominate: 1×1, 2×1, 3×1, 4×1, 3×3. This later structure has two different patterns to be called A and B respectively. The 3×3(A) structure in the literature is usually referred to as a $\sqrt{3}\times\sqrt{3}$ structure. This is due to the high degree of symmetry of the 3×3(A), so that a much smaller unit cell can be constructed. There is even a third 3×3 structure denoted as C which is degenerate with the 3×1 structure. In the following we shall try to explain briefly the gross features of the diagram. An important consideration to that respect is the evaluation of the numbers n_1 and n_2 respectively of the average number of first and second neighbours which have opposite displacements (in sign). The large relative displacements give large positive or negative contributions to the total energy. Of course, the measure of the relative displacements is important for distinguishing between patterns with the same n_1 and n_2 numbers. This depends not only on the average numbers (n_1 and n_2) over the whole unit cell,

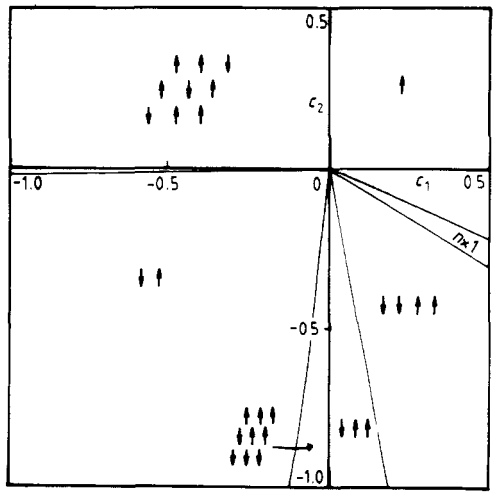

Figure 2. Ground state ($T=0$) phase diagram for the φ^4 potential. The on-site potential parameters are $g_0 = g_4 = 0.5$.

but also on the corresponding numbers for each specific atom. In table 3 we present the average n_1 and n_2 numbers for the different configurations.

For attractive first and second neighbours, $c_1 > 0$ and $c_2 > 0$, the lowest energy state is the 1×1 (ferro) with all the atoms in the minima at $u = u_0$ (or $u = -u_0$ for the degenerate state). The 1×1 persists even with repulsive second neighbours ($c_2 < 0$), where there is a triangular-shaped region containing 5×1, 6×1, 7×1, 8×1, 9×1 and 10×1 structures in an irregular manner.

Continuing clockwise there is a large region of 4×1 which has a large n_2 number which means that for repulsive second neighbours the energy is significantly lowered, while it overwhelms other structures with the same n_2 but with larger n_1, since $c_1 > 0$. For small $c_1 > 0$ and $c_2 < 0$, approximately between the lines $5c_2 + c_1 < 0$ and $c_1 = 0$ we find the 3×1 structure. Even though it has the same n_2 and higher n_1 numbers than the 4×1, it has lower energy because we must take into consideration also the magnitudes of the relative displacements between atoms in the region where c_1 becomes small. As shown in table 3 the 3×3(C) structure is degenerate in energy with the 3×1 structure, which has the same n_1 and n_2 numbers. On the other side of the negative c_2 axis we have the degenerate 3×3(B) and 3×3(B′) structures with $n_1 = 1.55$ and $n_2 = 2$ which overtake the 3×1 because n_1 is larger and $c_1 < 0$.

Table 3. The average number of first (n_1) and second (n_2) neighbours per site which present displacements with opposite signs.

Period	Structure	n_1	n_2
1×1	↑	0	0
2×1	↑ ↓	2	2
3×1	↑ ↑ ↓	1.33	2
4×1	↑ ↑ ↓ ↓	1	2
5×1	↑ ↑ ↑ ↓ ↓	4/5	8/5
$n \times 1$ ($n/2, n/2$)	↑ ↑ ↑ ↓ ↓ ↓	$4/n$	$8/n$
$n \times 1$ ($n-1, 1$)	↑ ↑ ↑ ↑ ↑ ↓	$4/n$	$6/n$
	↑ ↑ ↓	2	0
3×3(A)	↑ ↓ ↑ ↓ ↑ ↓		
$n \times n$	as in 3×3(A)	$6/n$	$4/n$
2×2	↑ ↓ ↑ ↑	1.5	1.5
3×3(B)	↑ ↑ ↑ ↓ ↑ ↑ ↓ ↓ ↓	1.55	2
3×3(B′)	↑ ↑ ↑ ↓ ↓ ↑ ↓ ↓ ↑	1.55	2
3×3(C)	↓ ↓ ↓ ↑ ↑ ↓ ↓ ↑ ↓	1.33	2
3×1(D)[a]	↑ • ↓	(4/3, 2/3)	(2, 1)
3×3(D)[a]	↑ ↓ • ↓ • ↑ • ↑ ↓	(2, 1)	0

[a] In these periodicities there are three different displacement so that the pair (2, 1) means that there are two neighbours like • ↑ or • ↓ and one neighbour like ↑ ↓ per atom on average.

In the $c_1, c_2 < 0$ region, the largest area is occupied by the 2×1 (antiferro) structure which has the highest possible values for both n_1 and n_2. In comparing the 2×1 and 4×1 structures from table 1 we see that their energies are equal on the negative c_2 axis ($c_1 = 0$).

The last quadrant of the phase diagram is occupied by the symmetric 3×3(A) configuration which has $n_1 = 2$ and $n_2 = 0$, thus overtaking 1×1 for $c_1 < 0$. The line $c_2 = 0$ is included in the area occupied by 3×3(A) which slowly extends to small but negative c_2. The boundary curve seems to be a parabola, its concave side facing $c_2 < 0$, although we have no analytic expression for the 3×3(A) structure, (as in the case of the DQ potential) to show it explicitly.

In our search for the ground state, we have compared the energies of periodicities up to 15×1 and 4×4 among themselves. At the borders of 3×1 with 4×1 and of 4×1 with $n \times 1$, we have, in small intervals of the phase space parameters, calculated energies up to the 40×1 periodicity. The borderlines separating large areas of periodic structures are not sharp. The periods of the structures within the boundaries of the main structures will be $p_1 + p_2$, $p_1 + 2p_2$, or $2p_1 + p_2$, if p_1 and p_2 are the periods of the structures that the borderline separates.

Finally in figure 3, for comparison we present the phase diagram for the DQ potential partly produced by directly comparing the analytical energy expressions and partly by the simulated annealing Monte Carlo method described previously. The simulated annealing method has more difficulties in converging to the lowest ground states for the same annealing pattern than in the φ^4 potential. Here we should mention that the simulated annealing results were smoothed out and only periodicities which occupy a large area in the c_1, c_2 space have been shown, in order to clearly present the differences between the DG and φ^4 potentials. Details are discussed in the last section. In the next section we will discuss the stability of the periodic structures which is quite different for the two potentials as can be seen from figures 2 and 3.

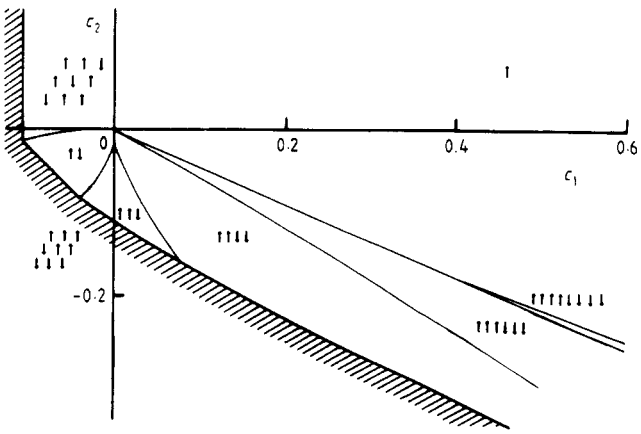

Figure 3. Ground state ($T = 0$) phase diagram for the double quadratic potential ($k^2 = 1$, $\sigma_0 = 1$).

To investigate the transition between different periodicities we give a contour plot of the energy as a function of c_1 and c_2 in figures 4(a) and 4(b) for φ^4 and DQ respectively. For the grid of investigation, the contours are quite smooth curves and they are parallel curves having the same slope. In the region where 4×1 and 2×1

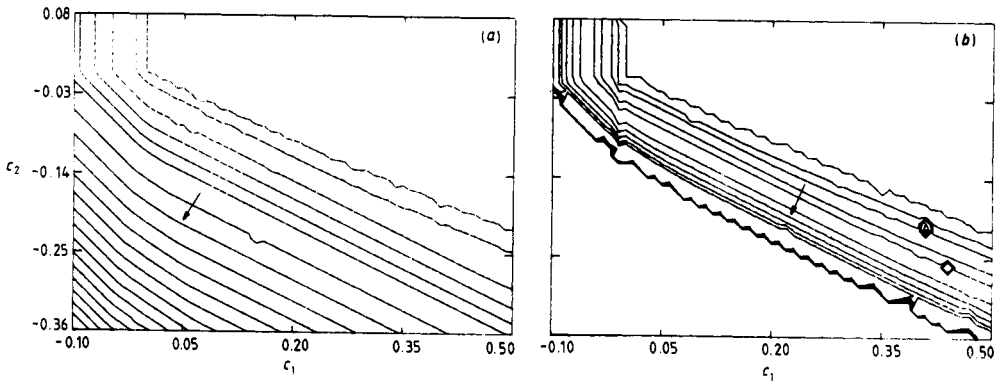

Figure 4. Contour plot of the ground-state energy as a function of c_1 and c_2 for (*a*) the φ^4 and (*b*) the DQ potential. The energy is decreasing in the direction of the arrow.

appear the slopes are $-\frac{1}{2}$ and -1 respectively as can also be seen from the explicit energy expressions in table 1. For the region where 3×3(A) is the ground state, the slope is infinite since there is no c_2 dependence in energy. In the 3×1 and 3×3(B) regions the contours are curved suggesting that the respective energies are not linear functions of c_1 and c_2. Of course, in the transition region between the different periodicities one expects a variety of commensurate structures, which on a smaller scale could show fluctuations in the energy contours of the ground state, and different curvatures. In the DQ case in fact, near the instabilitity region (see next section), the energy contours are very dense and show changes in curvature.

4. Stability

We review first the results for the DQ potential which can be valid also for the 1×1 structure for the φ^4 model. In the DQ model the stability is the same for all the periodic structures due to the piecewise linearity of the force. In checking for linear stability we look for a perturbation of the periodic solution $u^{(0)}_{n,m}$, i.e.

$$u_{n,m} = u^{(0)}_{n,m} + v_{n,m} \tag{7a}$$

with

$$v_{n,m} \approx \exp[\mathrm{i}(mp + nq - \omega t)] \tag{7b}$$

where (p, q) are the wavevector components in the first Brillouin zone, in the skew coordinate system. The system is stable if the linearised equations obtained by substituting (7*a*) in the equations of motion, have positive eigenvalues for all (p, q) in the Brillouin zone, i.e. if

$$B(p,q) = \frac{\omega^2(p,q)}{k^2}$$

$$= 1 - 2c_1[\cos p + \cos q + \cos(p-q) - 3]$$

$$- 2c_2[\cos(2p-q) + \cos(p-2q) + \cos(p+q) - 3] \tag{8}$$

is positive. To check this, it is only necessary to look for the minima of the dispersion surface. There are five families of minima points (see figure 5):

ferro F $(0, 0)$

antiferro AF $(0, \pm\pi), (\pm\pi, 0), (\pm\pi, \pm\pi)$

triagonal T $(2\pi/3, -2\pi/3), (-2\pi/3, 2\pi/3), (4\pi/3, 2\pi/3)$, etc

helical H_1 $(0, \pm q_1), (\pm q_1, 0), (q_1, q_1), (-q_1, -q_1)$

with $\cos q_1 = -(1 + c_1/c_2)/2$ for $-3 < c_1/c_2 < 1$

helical H_2 $(q_2, -q_2), (2q_2, q_2), (q_2, 2q_2)$

with $\cos q_2 = (1 - c_1/3c_2)/2$ for $-3 < c_1/c_2 < 9$.

The names used for the minima denote the symmetry of the corresponding periodic plane wave and the structure of the planar lattice, if the particular point of the dispersion is the lowest, i.e. ferro → 1×1, antiferro → 2×1, triagonal → 3×3(A). This type of 'soft mode' assumption is not unreasonable. In fact it is quite well satisfied for the DQ potential, with a 'weak' condition (Axel and Aubry 1981) on the signs of the $u_{n,m}$ ($\sigma_{n,m}$). The solution for the above cases is also consistent with the strong condition on $\sigma_{n,m}$ for the particular periodic structures. Other minima of the dispersion relation, i.e. the 'helical' points (which in magnetic systems correspond to rather interesting helical-type structures), do not impose their structure on the lattice. The corresponding periodic solution for the lattice does not necessarily have the lowest energy for that particular range of the phase space parameters c_1 and c_2. Of course, special 'helical' solutions can exist, i.e. the $n \times 1$ and $n \times m$ structures. In fact, $n \times 1$ structures are actually found along straight lines, as can be seen in figure 3, but the $n \times m$ periodicities do not give minima in the same region that the helical $n \times m$ points are minima.

Figure 6 shows the stability area for the DQ potential. What is remarkable here—although very special for this piecewise linear force—is that the static displacements $u^{(0)}_{n,m}$, together with the $\sigma_{n,m}$ parameters, do not appear in the expression for the frequency of the linearised perturbations, so that all structures have the same stability

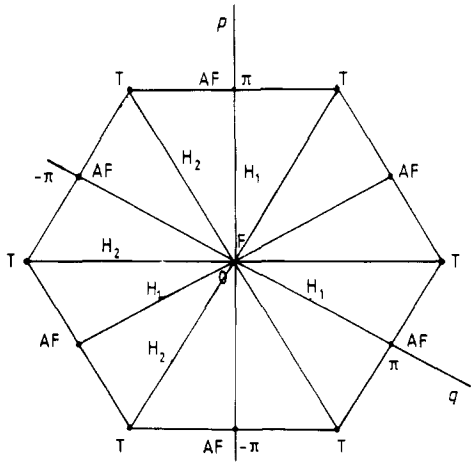

Figure 5. Minima of the dispersion relation, for the DQ potential, in the first Brillouin zone.

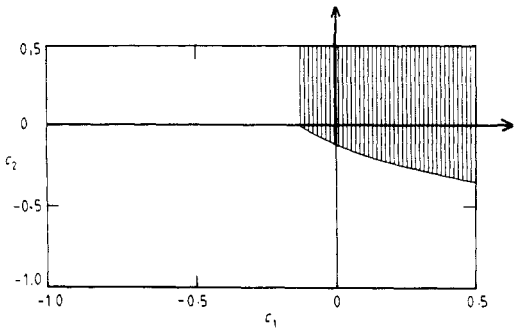

Figure 6. Stability area (strips) for the DQ potential and the 1×1 structure in φ^4.

region. Due to the nonlinearity of the φ^4 a general expression for the frequency of small oscillations is not possible for all configurations. Therefore we have to consider the stability of each periodic solution seperately.

The linearised equations for the φ^4 potential are:

$$\ddot{v}_{n,m} = f_1\Delta_6 v_{n,m} + f_2\Delta_6' v_{n,m} + g_0 v_{n,m} - 3g_4 u_{n,m}^{(0)2} v_{n,m}. \tag{9}$$

By substituting $u_{n,m}^{(0)} = \sqrt{g_0/g_4}$ and normalising the force constants to $2g_0$ we get for the 1×1 solution the same eigenvalue problem and the same $B(p, q)$ as above. (In (8) $k^2 \to 2g_0$.) We can also solve analytically for the stability of the 2×1 and 4×1 structures by substituting in (9) for the corresponding $u_{n,m}^{(0)}$ from table 1 and obtain for $B(p, q)$

$$B_{2\times1}(p, q) = 1 - 24(c_1 + c_2) - 2c_1[\cos p + \cos q + \cos(p-q) - 3]$$
$$- 2c_2[\cos(2p-q) + \cos(p-2q) + \cos(p+q) - 3] \tag{10}$$

$$B_{4\times1}(p, q) = 1 - 12(c_1 + 2c_2) - 2c_1[\cos p + \cos q + \cos(p-q) - 3]$$
$$- 2c_2[\cos(2p-q) + \cos(p-2q) + \cos(p+q) - 3]. \tag{11}$$

The above two expressions have the same (p, q) dependence (because of the square of $u_{n,m}^{(0)}$) and therefore the same extrema points. But since the dependence on c_1, c_2 is different the stability diagrams can be very different, as can be seen in figures 7(a) and (7b).

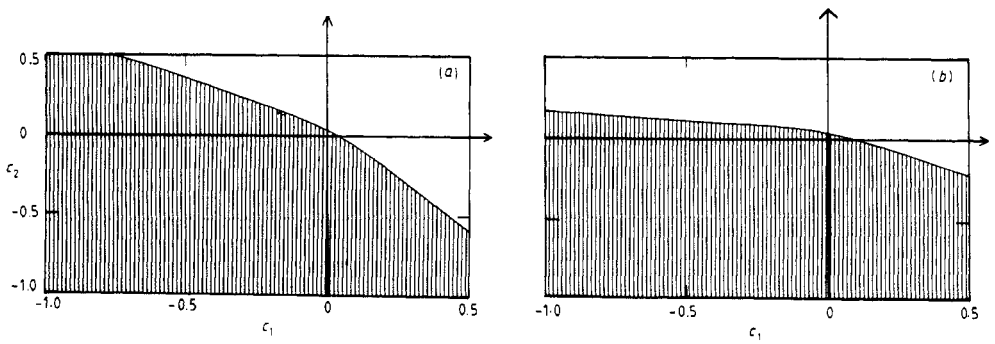

Figure 7. Stability area (strips) for (a) 2×1 and (b) 4×1 in the φ^4 model.

The investigation of the stability for the rest of the periodic structures appearing in the ground-state phase diagram, has to be done numerically for mainly two reasons. (i) The equilibrium displacements are not known analytically because equation (3) produces in general a system of nonlinear equations whose number can be as high as the total number of atoms in the unit cell. (ii) The Fourier-transformed linearised eigenvalue system of equations becomes quite large and it is not even clear that the eigenvalues have the same dependence on p and q. The matrix that gives the different branches of the spectrum involves the different displacements $u^{(0)}_{n,m}$. Therefore, one has to scan the whole Brillouin zone.

In this way the 3×1 and 3×3(A) stability analysis was done as shown in figures $8(a)$ and $8(b)$ respectively. For a general 3×3 structure we must solve a 9×9 matrix eigenvalue problem, which in the case of the 3×3(A) is reduced to a 3×3 matrix. For 5×1 and 6×1, stability was checked only in the $c_1>0$, $c_2<0$ region and for the 3×3(B) structure in the $c_1<0$, $c_2<0$ region. They were all found to be stable in the area in which they appear in the (c_1, c_2) phase diagram. In fact the same is true for all the

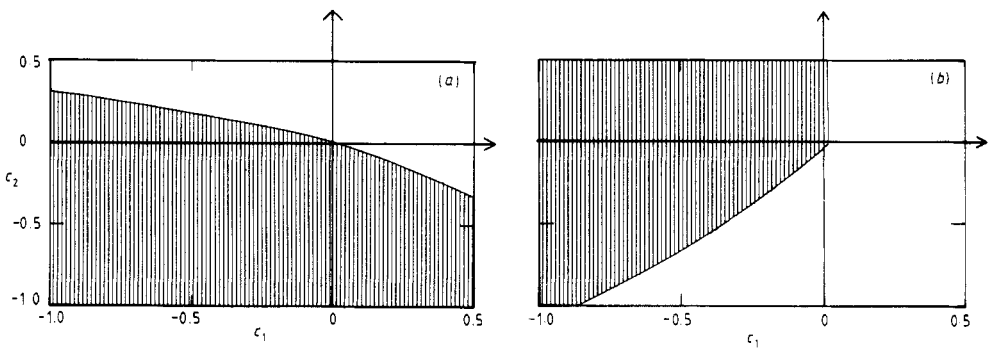

Figure 8. Stability area (strips) for (a) 3×1 and (b) 3×3(A) in the φ model.

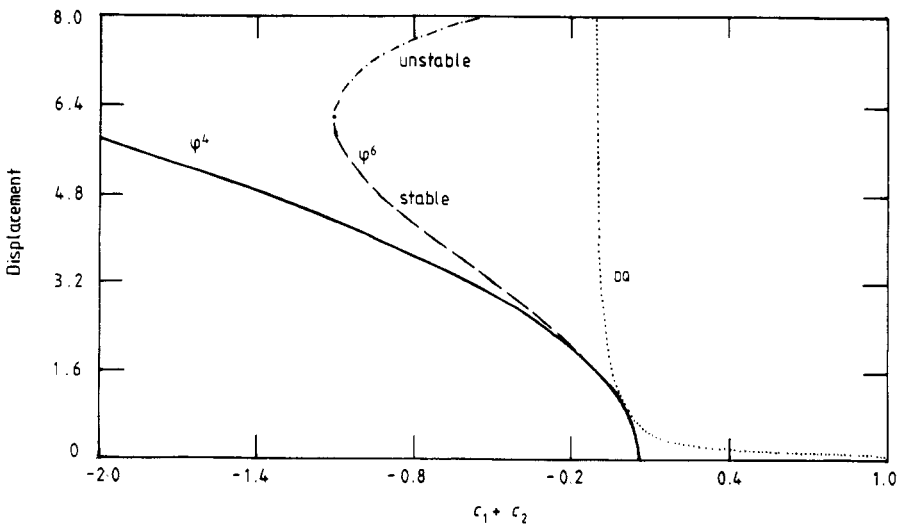

Figure 9. Plot of the displacement for the 2×1 structure as a function of c_1+c_2 for the DQ and φ^4 potentials. The curve for the φ^6 potential has both stable and unstable branches $g_6=\frac{1}{2}$.

periodicities checked. This is not surprising since the Monte Carlo method minimises the energy and should in principle find a global stable minimum. The only complication can arise from the imposition of periodic boundary conditions, which could act as an external constraining force if the periodicity of the ground-state structures is not the same as that of the structures examined.

5. Discussion

Using Monte Carlo numerical techniques, we determined the low-periodicity structures and constructed a phase diagram of the ground state at zero temperature. The grid in the space of the interaction parameters was quite coarse so that the boundaries are accurate only up to 10^{-2} in the normalised values of c_1 and c_2. This will give us a first approximate picture of the periodic structures that occupy the largest area in the (c_1, c_2) phase diagram.

In comparing the results for the two potentials there are both similarities and differences. The same commensurate phases appear for both potentials, but they cover different size areas in the space of the parameters (c_1, c_2). Thus in the φ^4 potential the 2×1 structure occupies essentially the whole $c_1, c_2<0$ quadrant, while in the DQ case it is limited near small c_1 and c_2 values. Similarly, the 3×3(A) structure occupies the whole $c_1<0$, $c_2>0$ quadrant for the φ^4 potential, while it is limited to a narrow strip parallel to the c_2 axis for the DQ case. These important differences are due to the fact that the stability of the structures for the DQ potential is strongly confined. Thus the region $c_1<0$, $c_2<0$ is practically not allowed, because the harmonic interparticle interactions are repulsive and the atoms can easily climb to large displacements along the also quadratic on-site potential driving thus the instability. In contrast for the φ^4 potential, the stability region of the nonlinear structures (different for each structure) covers the whole $c_1<0$ and $c_2<0$ area due to the steepness of the potential for large displacements. On the other hand the instability for an individual structure is caused when neighbouring atoms reach the top of the barrier at zero displacement. So, the actual form of the potential can be very important. We can expect more changes if we consider a softer potential for large displacement, like an inverted φ^6 potential, i.e.

$$V(u)=-\tfrac{1}{2}g_0u^2+\tfrac{1}{4}g_4u^4-\tfrac{1}{6}g_6u^6 \tag{12}$$

with $g_6>0$. The case $g_6<0$ will not significantly change the results of the φ^4. For $g_6>0$, however, we can demonstrate one change by looking at the 2×1 structure, where the displacement squared of the two oppositely displaced atoms in the unit cell is

$$u_0^2=\frac{g_4-\sqrt{g_4^2-4g_6[g_0-8(f_1+f_2)]}}{2g_6}. \tag{13}$$

There is a second solution with the positive sign in front of the square root which, however, is unstable, but for other periodicities it could give another possibility.

From equation (13) it is easy to show that there are no solutions for

$$f_1+f_2<\frac{g_0}{8}-\frac{g_4^2}{32g_6} \tag{14}$$

while for the φ^4 potential the solution extended for $f_1+f_2\to-\infty$. The new instability is caused by the softening of the potential at large displacements, which resembles the

DQ case (see conditions in table 2). The critical f_1+f_2 value also corresponds to the softening of the $(0, \pi)$ point in the Brillouin zone. On the large and positive side we still have the instability for $f_1+f_2 > g_0/8$ when the neighbouring atoms reach the top of the barrier. From the above we demonstrate the competition of the on-site potential and the interatomic interactions. The degree of softness of the on-site potential limits its region of stability. The softness of the DQ potential is also reflected in the sensitivity of the annealing procedure of the Monte Carlo method for the determination of the ground state. Thus, to obtain the diagram in figure 3 it was necessary, near the borderlines between structures, to repeat the procedure more than once. The $T=0$ phase diagram can also yield some information on what to expect at finite temperature (Janssen and Tjon 1982). By taking the thermal average of the equation of motion and using the self-consistent phonon approximation, i.e.

$$u_{n,m}^3 \approx 3\langle u_{n,m}^2 \rangle u_{n,m}$$

we obtain for the thermal average $\langle u_{n,m} \rangle$ the same equation as for $u_{n,m}$ except that the parameter g_0 becomes $g_0' = g_0 - 3\langle u_{n,m}^2 \rangle g_4$. So, decreasing the temperature, the fluctuations decrease and the effective g_0 increases. This means that in the (c_1, c_2) diagram (for the same f_1 and f_2), we move essentially parallel to the line $c_1 = c_2$ and from the upper-right corner to the lower-left corner. This picture, however, is very approximate. In fact, increasing the temperature or couplings tends to favour motion of the particle between the two minima and we can also have the appearance of a 'paramagnetic' or disordered phase. This would be reflected in the single-particle probability distribution with a transition from a two-hump function to a single peak at $u=0$. To obtain reliable phase diagrams, however, we need to consider explicitly the quantum mechanical free energy of the system (Frosch and Büttner 1985). This work is in progress.

In this paper we have not examined in detail the possibility of an incommensurate (IC) ground state. Of course there may also exist incommensurate phases and domain walls, but we will be concerned with these in later work. It is also difficult to eliminate numerically the possibility of a nearby long-periodicity structure. Some preliminary results are obtained by assuming that the IC state can be well represented by a sinusoidal modulation ansatz for the displacement (Behnkert *et al* 1987). This is a good assumption near the normal-to-IC phase transition but is not valid over the whole possible region of incommensurability (Janssen 1986a). For the parameters considered in our phase diagram (with a grid of 0.02) the IC state energy was higher than the lowest periodic structure. This is not in disagreement with the results of Benkert *et al* (1987) where the range of parameters for which an IC ground state was found corresponds, in our case, to a single-well on-site potential. This result is also not in contradiction with an analytical result of Axel and Aubry (1981), in a one-dimensional model, where it was assumed that the amplitude of modulation is very small, which again could correspond effectively to a potential with a single minimum. We plan a detailed study of the IC states (which we expect to be of limited extent in the range of parameters studied) also over a larger range of model parameters with a finer grid and using mapping techniques which, however, require large computations.

Finally we must look in more detail along the borderlines of figure 2. For sufficiently large on-site potential or equivalently small interatomic force constants the commensurate numbers are everywhere dense so that the incommensurate phase will be unstable with respect to nearby high-order commensurate structures. This, however, need not be the case for a weak potential. The point $c_1 = c_2 = 0$ also seems to be the meeting

point of many competing structures. Finally the work should be extended to study the nonlinear stability of the described ground states; that is, to consider the spontaneous creation of domains either as one-dimensional domain walls or as two-dimensional clusters with lower energy than the periodic structures.

Our results present similarities with the results of a triagonal Ising model with nearest- and next-nearest-neighbour interactions with an external field (Tanaka and Uryu 1975, Nakanishi and Shiba 1982). There are, however, qualitative and quantitative differences in the phase diagram. The main reason is that the external magnetic field tends to align all spins in one direction in the absence of interaction between spins. Thus the $c_1 = c_2 = 0$ point is not a multiple degeneracy point since only the 1×1 structure has the lowest energy. This causes both a shift of the structures towards negative c_1 and c_2 and also some rearrangements. The unidirectionality of the magnetic field is in contrast to the double-well potential, so that we expect quite different structures for the possible stable domain walls.

The phase diagram will change significantly for a different geometry of the 2D lattice since the important 'coordination' numbers n_1 and n_2 will be different. In particular, for a square lattice (Vlastou-Tsinganos and Flytzanis 1989) we have the ratio of $n_1/n_2 = \frac{1}{2}$ for each site. We also expect, for symmetry reasons, the 3×1 and 3×3 periodicities not to be important, as was actually found.

Our model is relevant to the description of the phases of biphenyl (Heine and Price 1985, Benkert *et al* 1987, Benkert 1987, Benkert and Heine 1987), where a φ^4 intramolecular potential is included. Also, the periodic structures of $LiIO_3$ have been already studied by (Coquet *et al* 1988) with a DQ potential with two degrees of freedom, describing the α and β phases and their transitions. An improvement of our model to two degrees of freedom with an inclusion of off-plane motion could be a good model for the γ-phase of $LiIO_3$.

Acknowledgments

The authors would like to thank M Peyrard for helpful discussions and G Grest for a discussion on the simulated annealing method. Part of this work is supported by EEC Stimulation programme ST2J-0032-1-GR.

References

Aubry S 1979 *Solitons and Condensed Matter Physics* ed A R Bishop and T Schneider (Berlin: Springer) p 264
Axel F and Abury S 1981 *J. Phys. C: Solid State Phys.* **14** 5433
Bak P 1982 *Rep. Prog. Phys.* **45** 587
Behnke G and Büttner H 1982 *J. Phys. A: Math. Gen.* **15** 3869
Behnke G, Bilz H and Büttner H 1986 *Phys. Rev. Lett.* **56** 1276
Benkert C 1987 *J. Phys. C: Solid State Phys.* **20** 3369
Benkert C and Heine V 1987 *Phys. Rev. Lett.* **58** 2232
Benkert C, Heine V and Simons E H 1987 *J. Phys. C: Solid State Phys.* **20** 3337
Bilz H, Benedek G and Bussmann-Holder A 1987 *Phys. Rev.* B **35** 4840
Bilz H, Bussmann A, Benedek G, Büttner H and Strauch D 1980 *Ferroelectrics* **25** 339
Büttner H and Heym J 1987 *Z. Phys.* B **68** 279
Coquet E, Peyrard M and Büttner H 1988 *J. Phys. C: Solid State Phys.* **21** 4895
Flytzanis N, Crowley S and Celli V 1979 *Phys. Rev. Lett.* **39** 891
Frosch H and Büttner H 1985 *J. Phys. C: Solid State Phys.* **18** 6303

Gordon M and Villain J 1985 *J. Phys. C: Solid State Phys.* **18** 3919
Heine V and Price S L 1985 *J. Phys. C: Solid State Phys.* **18** 5259
Janssen T 1986a *Incommensurate Phases in Dielectrics* vol 1, ed R Bline and A P Levanyuk (Amsterdam: North Holland)
Janssen T 1986b *Ferroelectrics* **66** 203
Janssen T and Tjon T 1982 *Phys. Rev.* B **25** 3767
Kanamori J and Okamoto M 1985 *J. Phys. Soc. Japan* **54** 4636
Katsura S, Ide T and Morita T 1986 *J. Stat. Phys.* **42** 381
Kirkpatrick S, Gellatt C D Jr and Vecchi M P 1983 *Science* **220** 671
Nakanishi K and Shiba H 1982 *J. Phys. Soc. Japan* **51** 2089
Srolovitz D J and Scott J F 1986 *Phys. Rev.* B **34** 1815
Tanaka Y and Uryu N 1975 *J. Phys. Soc. Japan* **39** 825
Takayanagi K, Tanishiro Y, Takahashi S and Takahashi M 1985 *Surf. Sci.* **169** 364
Vlastou-Tsinganos G and Flytzanis N 1989 *Singular Behavior and Nonlinear Dyanmics* ed St Pnevmatikos, T Bountis and Sp Pnevmatikos (Singapore: World Scientific) pp 419-35